Coherent-Error Threshold for Surface Codes from Majorana Delocalization

Florian Venn,[1,*] Jan Behrends,[2,*] and Benjamin Béri[1,2,†]

[1]*DAMTP, University of Cambridge, Wilberforce Road, Cambridge, CB3 0WA, United Kingdom*
[2]*T.C.M. Group, Cavendish Laboratory, University of Cambridge, J.J. Thomson Avenue, Cambridge, CB3 0HE, United Kingdom*

Statistical mechanics mappings provide key insights on quantum error correction. However, existing mappings assume incoherent noise, thus ignoring coherent errors due to, e.g., spurious gate rotations. We map the surface code with coherent errors, taken as X or Z rotations (replacing bit or phase flips), to a two-dimensional (2D) Ising model with complex couplings, and further to a 2D Majorana scattering network. Our mappings reveal both commonalities and qualitative differences in correcting coherent and incoherent errors. For both, the error-correcting phase maps, as we explicitly show by linking 2D networks to 1D fermions, to a $\mathbb{Z}_2$-nontrivial 2D insulator. However, beyond a rotation angle ϕ_{th}, instead of a $\mathbb{Z}_2$-trivial insulator as for incoherent errors, coherent errors map to a Majorana metal. This ϕ_{th} is the theoretically achievable storage threshold. We numerically find $\phi_{\mathrm{th}} \approx 0.14\pi$. The corresponding bit-flip rate $\sin^2(\phi_{\mathrm{th}}) \approx 0.18$ exceeds the known incoherent threshold $p_{\mathrm{th}} \approx 0.11$.

A major milestone toward building scalable quantum computers is quantum error correction (QEC) [1–3]. Surface codes are among the most promising candidates for this [4–8]. Their layout informs the design of state-of-the-art many-qubit devices [9], where most recent developments include proof-of-principle demonstrations of surface-code QEC on small systems [10,11].

Key insights on the phenomenology and fundamental performance limits of QEC codes come from mappings to statistical mechanics models [7,12–16]. For the surface code, assuming ideal measurements and either bit-flip X or phase-flip Z errors occurring with probability p, this is the two-dimensional (2D) random-bond Ising model (RBIM) [7,12]. The ordered and disordered RBIM phases map, respectively, to regimes where QEC succeeds and fails for large system size L, while the phase transition marks the theoretical maximum rate $p_{\mathrm{th}} \approx 0.11$ [17–19] of errors that can be corrected. (Tailoring the code for such biased noise may achieve higher thresholds [20].)

The RBIM mapping assumes incoherent errors. Coherent errors can, however, also arise, e.g., from unintended or imperfect gate rotations [21–32]. While results are favorable on their mitigation [23–25] or correction at fixed L [27,28], a key question for surface codes is how coherent errors' interference [30,31] impacts the scaling with L. Numerical results for either $\exp(i\phi X)$ or $\exp(i\phi Z)$ acting on each

qubit suggest that surface code QEC may succeed for $\phi < \phi_c \approx 0.1\pi$ [29]. While ϕ_c is decoder specific, $\sin^2(\phi_c) \lesssim p_{\mathrm{th}}$ suggests that assuming bit flips with $p = \sin^2(\phi)$ ("Pauli twirling") may work in practice. However, fundamental questions remain: What is the theory, replacing the RBIM, for the QEC phases? How does the phenomenology of these phases differ from the incoherent case? What is the maximum achievable threshold ϕ_{th}?

Here we introduce an RBIM that provides such a theory. Unlike probabilities of incoherent errors, quantum amplitudes now yield complex Boltzmann weights. Yet, the problem has two useful and interrelated [18,33–35] formulations, each encompassing both incoherent and coherent errors (cf. Fig. 1): a 2D Majorana network, and a 1D fermion Hamiltonian, both arising from the transfer matrix—a nonunitary quantum circuit akin to those of current interest in quantum dynamics [36].

We find that, upon increasing ϕ, the network undergoes an insulator-metal transition. This is qualitatively distinct from the incoherent case whose network, upon increasing p, has an insulator-insulator transition [18,37–42]. A key shared feature we find is that both the coherent and the small-p incoherent insulators are $\mathbb{Z}_2$ nontrivial: they correspond to topological 1D fermion phases [43]. We use this to show that correcting coherent errors can succeed for $\phi < \phi_{\mathrm{th}}$, with ϕ_{th} the value at the insulator-metal transition. We numerically find $\phi_{\mathrm{th}} \approx 0.14\pi$ for the geometry in Fig. 1. Remarkably, the Pauli-twirled probability $\sin^2(\phi_{\mathrm{th}}) \approx 0.18$ exceeds $p_{\mathrm{th}} \approx 0.11$ by 64%.

QEC ingredients.—Surface codes are stabilizer codes [3–8,44–46]. They encode logical qubits in the common $+1$ eigenspace of stabilizers $S_v^X = \prod_{j \in v} X_j$ at vertices v and $S_w^Z = \prod_{j \in w} Z_j$ at plaquettes w of the lattice, where we
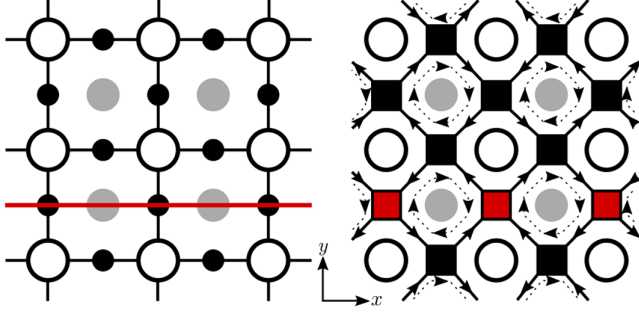
FIG. 1. Left panel: bulk patch of a surface code. Black dots are qubits, and white and gray disks, respectively, show stabilizers S_v^X and S_w^Z. The red line marks the logical $\overline{X}$'s path (for suitable boundary conditions). In the RBIM, the S_v^X become spins interacting with their nearest neighbors through couplings set by the errors. Right panel: in the network model, the Ising bonds become junctions scattering incoming into outgoing Majorana modes. Solid and dashed lines show, respectively, the modes' propagation direction for coherent and incoherent errors. In the transfer matrix, the junctions are quantum gates acting on pairs of Majorana operators.

multiply Pauli X and Z operators on qubits around v or w (cf. Fig. 1). The logical Pauli $\overline{X}_\gamma = \prod_{j\in\gamma} X_j$ and $\overline{Z}_{\gamma'} = \prod_{j\in\gamma'} Z_j$ run along noncontractible paths $\gamma^{(\prime)}$ such that they commute with all the stabilizers. The logical operators are not unique; their path can be deformed via multiplying by stabilizers. We focus on codes with a single logical qubit. We denote the logical operators along their shortest possible paths by $\overline{X}$ and $\overline{Z}$, and take L to be $\overline{X}$'s path length.

During the operation of the code, the constituent qubits can suffer errors. Here we focus on X errors, namely on the coherent $U = \prod_j e^{i\phi X_j}$, which we shall compare with incoherent bit flips X_j occurring with probability $p = \sin^2(\phi)$. (Z errors work similarly, upon $S_v^X, \overline{X} \leftrightarrow S_w^Z, \overline{Z}$ below.) Expanding U we find a superposition of X strings applied to the initial logical state $|\psi\rangle$. For a given string, the endpoints are where S_w^Z have eigenvalue $s_w = -1$. Starting from a string C_s consistent with the syndrome $s = \{s_w\}$, we can get all other such strings from multiplying by the S_v^X and/or $\overline{X}$. The former leaves $C_s|\psi\rangle$ unchanged; the latter takes it to $(C_s\overline{X})|\psi\rangle$. To correct errors, one measures s via the S_w^Z, and then applies either C_s or $C_s\overline{X}$ to return to the logical subspace [3]. In practice, this choice is made by a decoder. But if aiming for the theoretical optimum, one maximizes [32] $P_{q,s} = |\langle\psi|C_s\overline{X}^q U|\psi\rangle|^2$ over $q = 0, 1$. Henceforth, we take $|\psi\rangle$ to be a $\overline{Z}$ eigenstate; then, from $\overline{X}^q|\psi\rangle$ being orthogonal, $P_{q,s}$ are probabilities. The considerations in the incoherent case are similar, but instead of a superposition, we define $P_{q,s}$ for a probabilistic ensemble of strings [3,7]. In both cases, the probability of syndrome s is $P_s = \sum_q P_{q,s}$.

The feasibility of QEC hinges on $P_{0,s}$ and $P_{1,s}$ being sufficiently distinct. We measure this via

$$\Delta = \sum_s P_s \min_q \frac{P_{q,s}}{P_s} = \sum_s \min_q P_{q,s}. \qquad (1)$$

Besides its meaning for $\overline{Z}$ eigenstates $|\psi\rangle$, due to $P_{q,s} = \frac{3}{2} P_s \delta^{(q,s)}$ with $\delta^{(q,s)}$ the Bloch-sphere-averaged infidelity between pre- and post-QEC states [32], Δ also sets the minimal average infidelity. For incoherent errors, Δ is the logical error probability for maximum likelihood decoding [19]. The error correcting phase is defined by Δ decreasing to zero exponentially with L. Δ decaying to zero also marks the decoherence of logical noise [32,47].

From surface codes to Ising models.—To map our problem to an Ising model, we adapt the derivation of Ref. [7] to the coherent case [47]. In terms of the expansion of $U = \prod_j (\mathbb{1}\cos\phi + iX_j\sin\phi)$ in X strings, $\langle\psi|C_s\overline{X}^q U|\psi\rangle$ is the sum of the coefficients of $C_s\overline{X}^q \prod_v (S_v^X)^{r_v}$ for various configurations of $r_v \in \{0, 1\}$. (Other terms contribute to $U|\psi\rangle$ with states orthogonal to $C_s\overline{X}^q|\psi\rangle$.) In an N-qubit system, $C_s\overline{X}^q$ (i.e., all $r_v = 0$) has coefficient

$$(i\sin\phi)^n(\cos\phi)^{N-n} = \mathcal{N}\prod_j e^{-\eta_j^{(q,s)}J} \qquad (2)$$

with n the Pauli weight of $C_s\overline{X}^q$, $e^J = \sqrt{i\tan\phi}$, and $\mathcal{N} = \prod_j \sqrt{i\sin\phi\cos\phi}$; the signs are $\eta_j^{(q,s)} = -1$ if $C_s\overline{X}^q$ includes X_j, and $\eta_j^{(q,s)} = 1$ otherwise. We define Ising spins as $\sigma_v = -(-1)^{r_v}$. Since $\sigma_v\sigma_{v'} = 1$ for this term, and since each qubit is uniquely specified by nearest neighbor (NN) S_v^X (cf. Fig. 1; we use boundary conditions that also respect this [47]), Eq. (2) equals $\mathcal{N}\prod_{v,v'\text{NN}} e^{-J\eta_{vv'}^{(q,s)}\sigma_v\sigma_{v'}}$. (We relabeled $\eta_j^{(q,s)} \mapsto \eta_{vv'}^{(q,s)}$.) This holds also for other r_v configurations because, by $X_j^2 = \mathbb{1}$, a factor X_j comes from $\prod_v (S_v^X)^{r_v}$ only when $r_v = 1$ precisely for one v adjacent to j (thus $\sigma_v\sigma_{v'} = -1$), and this introduces X_j to $C_s\overline{X}^q$ when $\eta_j^{(q,s)} = 1$ and removes X_j when $\eta_j^{(q,s)} = -1$. Hence, $\langle\psi|C_s\overline{X}^q U|\psi\rangle = \mathcal{N}\mathcal{Z}_{q,s}$ with the Ising partition function

$$\mathcal{Z}_{q,s} = \sum_{\{\sigma_v\}} e^{-J\sum_{v,v'\text{NN}}\eta_{vv'}^{(q,s)}\sigma_v\sigma_{v'}}, \qquad e^J = \sqrt{i\tan\phi}. \qquad (3)$$

In the incoherent case, instead of terms in U we enumerate the probabilities of $C_s\overline{X}^q \prod_v (S_v^X)^{r_v}$ X strings; hence $i\sin\phi \mapsto p$, $\cos\phi \mapsto 1-p$ above and $P_{q,s} = \mathcal{N}\mathcal{Z}_{q,s}$. When sampling P_s by sampling C_s, this is the RBIM on the Nishimori line [7,48]. Equation (3) is our first key result.

2D networks and 1D Hamiltonians.—While $\mathcal{Z}_{q,s}$, being complex, might elude a direct statistical physics interpretation, valuable insights arise upon expressing it via the

transfer matrix $\hat{\mathcal{M}}_{q,s}$. It will be useful to construct $\hat{\mathcal{M}}_{q,s}$ along $\overline{X}$'s path, i.e., the x axis in Fig. 1. The steps being standard [47,49,50], we just state the result: $\mathcal{Z}_{q,s} = \langle \alpha_L | \hat{\mathcal{M}}_{q,s} | \alpha_0 \rangle$, with $| \alpha_r \rangle$ encoding boundary conditions at $x = r$, where $\hat{\mathcal{M}}_{q,s}$ is a quantum circuit

$$\hat{\mathcal{M}}_{q,s} = \hat{V}_{q,s}^{(L)} \hat{H}_{q,s}^{(L)} \dots \hat{V}_{q,s}^{(2)} \hat{H}_{q,s}^{(2)} \hat{V}_{q,s}^{(1)}. \qquad (4)$$

For system size M along y, $\hat{V}_{q,s}^{(k)} = \otimes_{j=1}^{M} \hat{v}_{q,s}^{(j,k)}$ and $\hat{H}_{q,s}^{(k)} = \otimes_{j=1}^{M} A_{q,s}^{(j,k)} \hat{h}_{q,s}^{(j,k)}$ in terms of gates $\hat{v}_{q,s}^{(j,k)}$ and $\hat{h}_{q,s}^{(j,k)}$ arising from the $(j,k)^{\text{th}}$ vertical and horizontal bond of the Ising model, respectively [here $A_{q,s}^{(j,k)} = \sqrt{2 \sinh(2J \eta_{jk}^{(q,s)})}$]. Upon a Jordan-Wigner transformation using $2M$ Majorana fermions $\hat{\gamma}_j = \hat{\gamma}_j^\dagger$, $\{\hat{\gamma}_i, \hat{\gamma}_j\} = 2\delta_{ij}$, we have $\hat{v}_{q,s}^{(j,k)} = e^{-i\kappa_{q,s}^{j,k} \hat{\gamma}_{2j} \hat{\gamma}_{2j+1}}$ ($j < M$) and $\hat{v}_{q,s}^{(M,k)} = e^{i\hat{P}\kappa_{q,s}^{M,k} \hat{\gamma}_{2M} \hat{\gamma}_1}$ with $\hat{P} = (-i)^M \hat{\gamma}_1 \hat{\gamma}_2 \dots \hat{\gamma}_{2M}$ the conserved fermion parity, and $\hat{h}_{q,s}^{(j,k)} = e^{-i\tilde{\kappa}_{q,s}^{j,k} \hat{\gamma}_{2j-1} \hat{\gamma}_{2j}}$. (We take $y \equiv y + M$, i.e., a cylinder; this can be argued to capture all key features [47].) Here $\kappa_{q,s}^{j,k} = J \eta_{jk}^{(q,s)}$, and $\tilde{\kappa}_{q,s}^{j,k} = -\frac{1}{2} \ln \tanh(J \eta_{jk}^{(q,s)})$.

The (nonunitary) gates $\hat{v}_{q,s}^{(j,k)}$ ($j < M$) and $\hat{h}_{q,s}^{(j,k)}$ act on NN fermions (cf. Fig. 1): they are quadratic in $\hat{\gamma}_j$. The same holds for $\hat{v}_{q,s}^{(M,k)}$, and hence also for $\hat{\mathcal{M}}_{q,s}$, for each of $P = \pm 1$. This has two key consequences. Firstly, we can write $\hat{\mathcal{M}}_{q,s} \hat{\mathcal{M}}_{q,s}^\dagger = e^{-L \hat{\mathcal{H}}_{q,s}}$ as a thermal density matrix, at inverse temperature L, with 1D Hamiltonian $\hat{\mathcal{H}}_{q,s}$ that is free fermionic for each of $P = \pm 1$ [51]. Taking $L \varepsilon_{q,s}^{(1)} \gg 1$ (with $\varepsilon_{q,s}^{(1)}$ the smallest excitation energy) yields the ground state $|\varphi_0\rangle$ which, by the singular value decomposition of $\hat{\mathcal{M}}_{q,s}$, is the steady state of the circuit Eq. (4) [47]. We shall link the topology of $|\varphi_0\rangle$ to error correction.

Secondly, the $2M \times 2M$ matrix $\mathcal{M}_{q,s}$, implementing $\hat{\mathcal{M}}_{q,s} \hat{\gamma}_j \hat{\mathcal{M}}_{q,s}^{-1} = (\mathcal{M}_{q,s})_{lj} \hat{\gamma}_l$, arises from a network of 2×2 matrices $v_{q,s}^{(j,k)} = e^{2Y\kappa_{q,s}^{j,k}}$ ($j < M$), $v_{q,s}^{(M,k)} = e^{-2PY\kappa_{q,s}^{M,k}}$ with $P = \pm 1$, and $h_{q,s}^{(j,k)} = e^{2Y\tilde{\kappa}_{q,s}^{j,k}}$ (here $Y = iXZ$). In the incoherent case, as J is real, these are pseudounitary [18]: $t^\dagger Z t = Z$, with $t = v_{q,s}^{(j,k)}$ or $t = h_{q,s}^{(j,k)}$. One can thus interpret them as acting on a pair $c = \binom{c_n}{c_{n+1}}$ of counterpropagating modes, conserving their current $c^\dagger Z c$. The RBIM thus maps to quantum transport [18,37–42,52]: we get a Chalker-Coddington network model [53], with $h_{q,s}^{(j,k)}$ and $v_{q,s}^{(j,k)}$ as junction transfer matrices (cf. Fig. 1). The junction scattering matrices, mapping incoming to outgoing amplitudes $\binom{\text{in}_n}{\text{in}_{n+1}}$ and $\binom{\text{out}_n}{\text{out}_{n+1}}$, in suitable phase conventions, are $S_h = \binom{a \ b}{b \ -a}$ and $S_v = \binom{-b \ a}{a \ b}$ with $a = \text{sech}(2\kappa_{q,s}^{j,k})$, $b = \tanh(2\kappa_{q,s}^{j,k})$ [18,40,42].

We find a different network in the coherent case. From $\tilde{\kappa}_{q,s}^{(j,k)} = i\phi - \frac{1}{2} \ln[-\eta_{jk}^{(q,s)}]$, the $h_{q,s}^{(j,k)}$ are unitary. This conserves $c^\dagger c$; this is the current if c has copropagating modes. Furthermore, now $X v_{q,s}^{(j,k)}$ is pseudounitary: If c's modes counterpropagate, $v_{q,s}^{(j,k)}$ swaps their direction. Equivalently, $v_{q,s}^{(j,k)}$ has a pair of vertically copropagating modes. In the coherent case, thus, both $h_{q,s}^{(j,k)}$ and $v_{q,s}^{(j,k)}$ have copropagating modes, moving horizontally and vertically, respectively (cf. Fig. 1). In a suitable phase convention, the scattering matrices are $S_\rightarrow = -\eta_{jk}^{(q,s)} \binom{\cos(2\phi) \ \sin(2\phi)}{-\sin(2\phi) \ \cos(2\phi)}$, $S_\leftarrow = S_\downarrow = S_\rightarrow^\dagger$, and $S_\uparrow = -S_\downarrow$, with arrows for the transmission direction, and $\binom{\text{out}_n}{\text{out}_{n+1}} = S_\alpha \binom{\text{in}_n}{\text{in}_{n+1}}$ with n increasing along y for $\alpha = \leftarrow, \rightarrow$ and along x for $\alpha = \uparrow, \downarrow$.

Their scattering matrices being real, both networks belong to Altland and Zirnbauer's symmetry class D [54], with links interpretable as Majorana modes. We will also consider the networks together with their time-reversed copies. This gives time-reversal invariant networks in class DIII. Viewed as such, the incoherent and coherent cases correspond to, respectively, the spin-conserving and spin-flip limits of the class DIII networks of Ref. [55], albeit with $\eta_{jk}^{(q,s)}$ creating a different form of disorder.

This disorder has the same net effect in the incoherent and coherent cases: $\eta_{jk}^{(q,s)} = -1$ adds a "vortex" at each of the adjacent S_w^Z (cf. Fig. 1): a mode encircling either of these picks up an extra π phase. With several $\eta_{jk}^{(q,s)} = -1$, vortices appear where $s_w = -1$. Vortices are thus the network form of the syndrome s.

Network model phases.—In the incoherent case, the network is known to have two insulating (i.e., localized) phases with a transition at $p_{\text{th}} \approx 0.11$ [18,38–40,42]. Being insulators, the average conductivity $g = (L/M) \langle \text{Tr}(\mathcal{T}^\dagger \mathcal{T}) \rangle$ satisfies $g \propto e^{-2L/\xi}$ for $L \gg \xi$; here $\langle \dots \rangle$ denotes disorder average, $\mathcal{T}$ is the transmission matrix in the transmission-reflection grading of the total scattering matrix $\mathcal{S} = \binom{\mathcal{R} \ \mathcal{T}'}{\mathcal{T} \ \mathcal{R}'}$ [56], and ξ is the localization length. The two insulators are topologically distinct: for $\mathcal{Q} = \text{sgn} \det(\mathcal{R}'_{\text{PBC}} \mathcal{R}'_{\text{APBC}})$, equal to the $\mathbb{Z}_2$ invariant of the doubled class DIII system [34,47,55], and where (A)PBC denotes (anti)periodic boundary conditions in the transverse direction, we have $\mathcal{Q} = \text{sgn}(p - p_{\text{th}})$ [18,55].

In the coherent case, we focus on $0 \le \phi \le \pi/4$; this includes all inequivalent ϕ values [57]. In the clean case (i.e., all $\eta_{jk}^{(q,s)} = 1$), any $\phi < \pi/4$ gives a $\mathcal{Q} = -1$ insulator [55]. With disorder, we now argue that the system remains insulating for $0 < \phi \ll 1$. We first note that if vortices typically appear in dilute configurations of nearby pairs, then, by the splitting of vortex-induced zero modes, a nearly decoupled network (i.e., with $\phi, p \ll 1$ nodes) is an insulator [40]. The typical vortex configurations for $\phi \ll 1$ are similar to the $p \ll 1$ incoherent case: there, for a
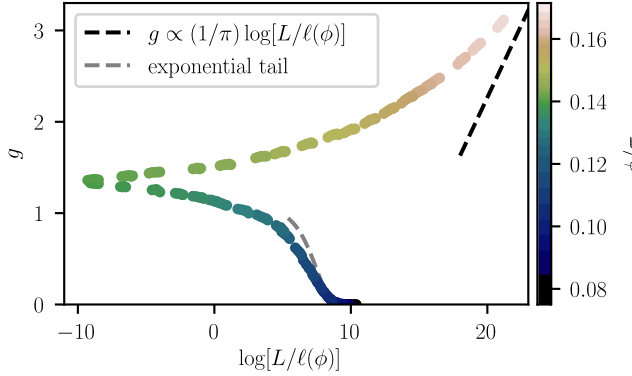
FIG. 2. Conductivity g for the coherent-error network on a cylinder of length L and circumference $M = 5L$, averaged over 500 to 10^5 syndrome realizations. Error bars ($2 \times$ standard error) are imperceptible. The data following scaling curves $g[L/\ell(\phi)]$ shows that ϕ enters via a length scale $\ell(\phi)$ [47]. For the insulator, $g[L/\ell(\phi)]$ decays with L and $g \propto e^{-2L/\ell(\phi)}$ for $L \gg \ell(\phi)$. For the metal, g increases; the $g \propto \ln(L)/\pi$ class D asymptote [37,42] is not yet reached for the accessible range of L. The insulator-metal transition is at $\phi_{\text{th}} = (0.14 \pm 0.005)\pi$. We observe $\mathcal{Q} = -1$ throughout the insulating phase.

FIG. 3. Figure of merit Δ for the $L \times L$ planar geometry of recent experiments [10,11] (cf. inset for $L = 3$, 5). We averaged over 250 to 2×10^5 syndrome realizations; error bars ($2 \times$ standard error) are imperceptible. Δ decays exponentially (dashed) with L for $\phi < \phi_{\text{th}}$. Above ϕ_{th}, the data are consistent with Δ decaying as a power law to $\Delta_\infty(\phi) < \Delta_{\text{u}} = (\pi - 2)/2\pi$.

configuration s with $\omega \ll LM$ adjacent vortex pairs (AVP), hence low AVP density $n_\omega = \omega/LM$, we have $P_s \propto p^\omega (1 - p)^{LM - \omega}$. There are $\sim \binom{LM}{\omega}$ such s with similar P_s. Thus ω has roughly binomial distribution. Hence, $\langle n_\omega \rangle \propto p$ with variance $\sigma_{n_\omega}^2 \propto p/LM$ suppressed for large LM. Among the s at $n_\omega \approx p$, those with a nonzero density of farther separated vortex pairs (from AVP chains) give just a $\propto e^{-cpLM}$ ($c > 0$) fraction of configurations. In the coherent case, $|\sum_j a_j| \leq \sum_j |a_j|$ gives $|\mathcal{Z}_{q,s}| \leq \mathcal{Z}_{q,s}(i \sin \phi \mapsto \sin \phi)$; the latter is the incoherent $\mathcal{Z}_{q,s}$ with $p \mapsto \sin \phi$, $1 - p \mapsto \cos \phi$ (not the Pauli twirl). Hence $P_s \lesssim (\sin^2 \phi)^\omega (\cos^2 \phi)^{(LM - \omega)}$ for $\phi \ll 1$. From here, the previous logic applies: Vortices typically appear in nearby pairs. Hence, the system insulates for $0 < \phi \ll 1$. Since $\mathcal{Q}$ cannot change without delocalization [47], and since $\mathcal{Q} = -1$ for $\phi = 0$ (a clean system), this small-ϕ insulator has $\mathcal{Q} = -1$. As we shall show, this implies that QEC succeeds up to a nonzero ϕ_{th}.

As ϕ increases, vortices proliferate. Generically, this gives a metal [40], the phase we expect beyond ϕ_{th}. (For the RBIM, J being real precludes a metal [38].) To test this and find ϕ_{th}, we study g for vortices drawn from P_s, sampling using Ref. [29]'s algorithm [47]. Our results are in Fig. 2. The $\mathcal{Q} = -1$ insulator persists up to $\phi_{\text{th}} = (0.14 \pm 0.005)\pi$, followed by a metal for $\phi > \phi_{\text{th}}$. Both phases show single-parameter scaling: ϕ enters only via a length scale $\ell(\phi)$. [For an insulator, $\ell(\phi) = \xi(\phi)$.] While this qualitatively agrees with class D results [58,59], for the metal $g[L/\ell(\phi)]$ increases slower toward $\pi^{-1} \ln[L/\ell(\phi)]$ than predicted by the nonlinear σ model (the standard theory for the metallic phase [37,38,42]). Establishing the insulator-metal phase diagram and ϕ_{th} are among our key results. Conceptually, the network

model phases offer coherent-error QEC phenomenology akin to how RBIM phases do in the incoherent case. Practically, since dg/dL, unlike $d\Delta/dL$ below, changes sign at ϕ_{th}, the network model greatly facilitates identifying ϕ_{th}.

From insulators to QEC.—We now establish ϕ_{th} as the coherent-error threshold. For this, we consider $\zeta_s = (\mathcal{Z}_{1,s}/\mathcal{Z}_{0,s})$. In the Ising language, ζ_s is a disorder correlator [47,60] since $\mathcal{Z}_{1,s}$ differs from $\mathcal{Z}_{0,s}$ by a row of sign-flipped bonds. We have $\zeta_s \propto e^{-\frac{1}{2}[E_{1,s}^{(0)} - E_{0,s}^{(0)}]L}$ for large L, with $E_{q,s}^{(0)}$ the lowest energy of $\hat{\mathcal{H}}_{q,s}$ [47]. To evaluate ζ_s, we consider the 1D free-fermion Hamiltonians that $\hat{\mathcal{H}}_{q,s}$ gives for each P. These Hamiltonians have gap $\propto \xi^{-1}$ if the corresponding network is an insulator and their ground state has fermion parity $\nu \text{sgn}[\det(\mathcal{R}')]$ (with $\nu = \pm 1$ set by $\mathcal{R}'$ conventions) [18,47]. The latter fact not only allows one to view $\mathcal{Q}$ as their 1D topological invariant [34,43,47], but, crucially, also implies that their number n of excitations satisfies $(-1)^n = \nu \text{sgn}[\det(\mathcal{R}')]P$.

Since each flips a row of vertical bonds, P and q effectively swap PBC and APBC for fermions. This is crucial when the network is a $\mathcal{Q} = -1$ insulator: from the $\det(\mathcal{R}')$ swapping sign, $\nu \text{sgn}[\det(\mathcal{R}')] = \chi_C (-1)^q P$, with $\chi_C = \pm 1$ set by C_s [47]. Thus $(-1)^n = \chi_C (-1)^q$, and $E_{1,s}^{(0)} - E_{0,s}^{(0)} \approx \chi_C/\xi$ up to $O(e^{-M/\xi})$ corrections from APBC vs PBC energy differences. Hence, $\zeta_s \propto e^{-\chi_C L/2\xi}$, and $\Delta \propto e^{-zL/2\xi}$, with $z = 2$ in the coherent and $z = 1$ in the incoherent case (from $P_{q,s} \propto |\mathcal{Z}_{q,s}|^z$). The $\mathcal{Q} = -1$ insulator thus marks the error correcting phase. [For a $\mathcal{Q} = 1$ insulator, $E_{1,s}^{(0)} - E_{0,s}^{(0)} = O(e^{-M/\xi})$: here QEC fails.] This establishes ϕ_{th} as the coherent QEC threshold.

Figure 3 shows numerical results on Δ for the planar geometry of recent $L = 3$, 5 experiments [10,11]. Our

theory describing this system shows that our predictions hold beyond the cylinder [47]: ϕ_{th} reflects bulk physics.

QEC in the metallic phase.—The metal for $\phi > \phi_{th}$, instead of the $\mathcal{Q} = 1$ insulator, is a qualitatively new feature. While the $\mathcal{Q} = 1$ insulator maps to a disordered phase [7,18], the metal, if we generalize metallic disorder correlator results [38], suggests a new QEC analog of quasi-long-range order where Δ decays nonexponentially with L. This is indeed what is seen in Fig. 3. The data are consistent with $\Delta = \lambda L^{-d_\Delta} + \Delta_\infty$, where $\lambda, d_\Delta, \Delta_\infty > 0$ depend on ϕ. Furthermore, we find $\Delta_\infty < \Delta_u = (\pi - 2)/2\pi$, the value for uniform ϕ_s in the logical $U_s = \exp(i\phi_s \overline{X})$ arising from QEC in this geometry [29,32].

Conclusion.—We have mapped surface codes with $\exp(i\phi X)$ [or $\exp(i\phi Z)$] coherent errors to a complex RBIM, and via its transfer matrix $\hat{\mathcal{M}}_{q,s}$, to quantum transport in a 2D Majorana network. The network yielded an insulator-metal phase diagram. Linking the insulator's $\mathbb{Z}_2$ invariant to the topology of 1D fermions, we explicitly mapped the insulator to the error-correcting phase and established the insulator-metal transition, at $\phi_{th} \approx 0.14\pi$, as the achievable storage threshold. Such a high achievable threshold, with $\sin^2(\phi_{th}) \approx 0.18 > p_{th} \approx 0.11$, explains why standard decoders, even if not optimal, can reach thresholds ϕ_c with $\sin^2(\phi_c) \lesssim p_{th}$ as in Refs. [29,32].

The metal we found highlights fundamentally distinct coherent-error physics. It maps to a new phase in QEC where, albeit as a power law and to a nonzero Δ_∞ value, Δ decays with L (Fig. 3). This is markedly different from the incoherent case where, above threshold, Δ increases and saturates exponentially with L [19].

*These authors contributed equally to this work.
†bfb26@cam.ac.uk

[1] A. R. Calderbank and P. W. Shor, Phys. Rev. A **54**, 1098 (1996).
[2] A. M. Steane, Phys. Rev. Lett. **77**, 793 (1996).
[3] B. M. Terhal, Rev. Mod. Phys. **87**, 307 (2015).
[4] A. Y. Kitaev, in *Quantum Communication, Computing, and Measurement* (Springer, New York, 1997), pp. 181–188.
[5] A. Y. Kitaev, Ann. Phys. (N.Y.) **303**, 2 (2003).
[6] S. B. Bravyi and A. Y. Kitaev, arXiv:quant-ph/9811052.
[7] E. Dennis, A. Kitaev, A. Landahl, and J. Preskill, J. Math. Phys. (N.Y.) **43**, 4452 (2002).
[8] A. G. Fowler, M. Mariantoni, J. M. Martinis, and A. N. Cleland, Phys. Rev. A **86**, 032324 (2012).
[9] F. Arute et al., Nature (London) **574**, 505 (2019).
[10] S. Krinner et al., Nature (London) **605**, 669 (2022).
[11] Google Quantum AI, Nature (London) **614**, 676 (2023).
[12] C. Wang, J. Harrington, and J. Preskill, Ann. Phys. (Amsterdam) **303**, 31 (2003).
[13] H. G. Katzgraber, H. Bombin, and M. A. Martin-Delgado, Phys. Rev. Lett. **103**, 090501 (2009).
[14] H. Bombin, R. S. Andrist, M. Ohzeki, H. G. Katzgraber, and M. A. Martin-Delgado, Phys. Rev. X **2**, 021004 (2012).
[15] A. Kubica, M. E. Beverland, F. Brandão, J. Preskill, and K. M. Svore, Phys. Rev. Lett. **120**, 180501 (2018).
[16] C. T. Chubb and S. T. Flammia, Ann. Henri Poincaré D **8**, 269 (2021).
[17] A. Honecker, M. Picco, and P. Pujol, Phys. Rev. Lett. **87**, 047201 (2001).
[18] F. Merz and J. T. Chalker, Phys. Rev. B **65**, 054425 (2002).
[19] S. Bravyi, M. Suchara, and A. Vargo, Phys. Rev. A **90**, 032326 (2014).
[20] D. K. Tuckett, S. D. Bartlett, S. T. Flammia, and B. J. Brown, Phys. Rev. Lett. **124**, 130501 (2020).
[21] R. Kueng, D. M. Long, A. C. Doherty, and S. T. Flammia, Phys. Rev. Lett. **117**, 170502 (2016).
[22] J. J. Wallman, arXiv:1511.00727.
[23] J. J. Wallman and J. Emerson, Phys. Rev. A **94**, 052325 (2016).
[24] D. M. Debroy, M. Li, M. Newman, and K. R. Brown, Phys. Rev. Lett. **121**, 250502 (2018).
[25] A. Hashim et al., Phys. Rev. X **11**, 041039 (2021).
[26] D. Greenbaum and Z. Dutton, Quantum Sci. Technol. **3**, 015007 (2017).
[27] S. J. Beale, J. J. Wallman, M. Gutiérrez, K. R. Brown, and R. Laflamme, Phys. Rev. Lett. **121**, 190501 (2018).
[28] E. Huang, A. C. Doherty, and S. Flammia, Phys. Rev. A **99**, 022313 (2019).
[29] S. Bravyi, M. Englbrecht, R. König, and N. Peard, npj Quantum Inf. **4**, 55 (2018).
[30] J. K. Iverson and J. Preskill, New J. Phys. **22**, 073066 (2020).
[31] D. Gottesman, arXiv:1907.05950.
[32] F. Venn and B. Béri, Phys. Rev. Res. **2**, 043412 (2020).
[33] I. C. Fulga, F. Hassler, A. R. Akhmerov, and C. W. J. Beenakker, Phys. Rev. B **83**, 155429 (2011).
[34] I. C. Fulga, F. Hassler, and A. R. Akhmerov, Phys. Rev. B **85**, 165409 (2012).
[35] C.-M. Jian, B. Bauer, A. Keselman, and A. W. W. Ludwig, Phys. Rev. B **106**, 134206 (2022).
[36] M. P. A. Fisher, V. Khemani, A. Nahum, and S. Vijay, Annu. Rev. Condens. Matter Phys. **14**, 335 (2023).
[37] T. Senthil and M. P. A. Fisher, Phys. Rev. B **61**, 9690 (2000).
[38] N. Read and A. W. W. Ludwig, Phys. Rev. B **63**, 024404 (2000).
[39] I. A. Gruzberg, N. Read, and A. W. W. Ludwig, Phys. Rev. B **63**, 104422 (2001).
[40] J. T. Chalker, N. Read, V. Kagalovsky, B. Horovitz, Y. Avishai, and A. W. W. Ludwig, Phys. Rev. B **65**, 012506 (2001).
[41] F. Merz and J. T. Chalker, Phys. Rev. B **66**, 054413 (2002).
[42] F. Evers and A. D. Mirlin, Rev. Mod. Phys. **80**, 1355 (2008).

[43] A. Y. Kitaev, Phys. Usp. **44**, 131 (2001).

[44] D. Gottesman, Phys. Rev. A **54**, 1862 (1996).

[45] A. R. Calderbank, E. M. Rains, P. W. Shor, and N. J. A. Sloane, Phys. Rev. Lett. **78**, 405 (1997).

[46] D. Gottesman, Stabilizer codes and quantum error correction, Ph.D. thesis, California Institute of Technology, 1997.

[47] See Supplemental Material at http://link.aps.org/supplemental/10.1103/PhysRevLett.131.060603 for further details on the Ising mapping, boundary conditions, network models, the 2D insulator-1D gapped fermion correspondence, the syndrome sampling, and on the link between 1D fermions, Δ, disorder correlators, and the decoherence of logical errors. It also includes raw conductivity data.

[48] H. Nishimori, Prog. Theor. Phys. **66**, 1169 (1981).

[49] S. Sachdev, *Quantum Phase Transitions*, 2nd ed. (Cambridge University Press, Cambridge, U.K., 2011).

[50] E. Fradkin, *Field Theories of Condensed Matter Physics* (Cambridge University Press, Cambridge, U.K., 2013).

[51] For boundary conditions allowing $\bar{X}$ along the cylinder, the $|\alpha_r\rangle$ are also free-fermion states [47].

[52] S. Cho and M. P. A. Fisher, Phys. Rev. B **55**, 1025 (1997).

[53] J. Chalker and P. Coddington, J. Phys. C **21**, 2665 (1988).

[54] A. Altland and M. R. Zirnbauer, Phys. Rev. B **55**, 1142 (1997).

[55] I. C. Fulga, A. R. Akhmerov, J. Tworzydło, B. Béri, and C. W. J. Beenakker, Phys. Rev. B **86**, 054505 (2012).

[56] C. W. J. Beenakker, Rev. Mod. Phys. **69**, 731 (1997).

[57] This is due to the QEC problem being equivalent (upon $X_j \mapsto -X_j$) for ϕ and $-\phi$, and being related by a q, s-independent factor $\prod_j X_j$ for ϕ and $\phi + \pi/2$.

[58] M. V. Medvedyeva, J. Tworzydło, and C. W. J. Beenakker, Phys. Rev. B **81**, 214203 (2010).

[59] T. Wang, Z. Pan, T. Ohtsuki, I. A. Gruzberg, and R. Shindou, Phys. Rev. B **104**, 184201 (2021).

[60] E. Fradkin, J. Stat. Phys. **167**, 427 (2017).